Contents lists available at ScienceDirect

Nuclear Engineering and Design

journal homepage: www.elsevier.com

Modelling flood propagation in the service galleries of a nuclear power plant

Ernest Bladé [a], Marcos Sanz-Ramos [a, *], Josep Dolz [a], Juan Manuel Expósito-Pérez [b], Martí Sánchez-Juny [a]

[a] Flumen Institute (UPC-CIMNE), E.T.S. d'Enginyeria de Camins, Canal i Ports de Barcelona, Universitat Politècnica de Catalunya – Barcelona TECH, C/Gran Capitán S/N, 08034 Barcelona, Spain

[b] IDOM S.A., Gran Via de Carles III 97, Bajos, 08028 Barcelona, Spain

ARTICLE INFO

Keywords:
ESWS
Urban drainage
Occupation index
2D hydraulic modelling

ABSTRACT

In the context of the stress tests that have to be applied to nuclear power plants, this work presents the study of the flooding processes of the service galleries of a nuclear plant caused by a hypothetical failure of some of the pipes of the Essential Services Water System (ESWS). To assess the flood propagation along the galleries, two-dimensional hydraulic modelling tools, based on the solution of the shallow water equations with the finite volume method, were used. Due to the complexity and special features of the geometry and hydraulic processes, when compared with more standard urban flood assessment works, several specific modules were developed. A relevant one is a new module to consider the effect of the occupation of the galleries on the advance of the waterfront. This module was developed and verified prior to being applied to a case study. The results show the suitability of the proposed methodology to be used as part of the stress tests to ensure high security standards of nuclear power plants.

1. Introduction

Nuclear power plants (NPPs) are electric power facilities that need greater attention regarding safety aspects than other kinds of power plants. The growing concern for safety, combined with the concerns arising from the aging of the facilities or changes in external conditions, has led international and national agencies to re-evaluate the security systems of these plants (Bunn and Heinonen, 2011; NERH, 2011; Wang and Chen, 2012). As a part of this safety analysis, failure caused by extreme geoclimatic agents such as hurricanes, earthquakes, floods, etc., has to be considered. In this sense, nuclear power plants have safety and safeguarding systems to minimize the possible negative effects of such events (Chen et al., 2017; Chiang et al., 2017; D'Auria et al., 2017). Since the Fukushima incident (Saji, 2014), national and international authorities have been analysing and evaluating the current state of the NPPs around the world. Among these actions, several stress tests have had to be applied in order to assess how safe the facility is. These tests were defined as a re-assessment of the safety thresholds regarding specific extreme natural hazards (e.g. COM, 2012). As a result, several recommendations, laws and directives have been modified or/and created looking for more effective actions on NPPs safety.

Under flooding events, nuclear power facilities normally have drainage systems that help to reduce and control the flood extension and the volume of water (Chen et al., 2017; USNRC, 2011). In the case of earthquakes, the safety systems on the essential elements (first and second order) are designed to allow the plant to continue working or, in case of a serious event, stop the plant activity under safe conditions (Nöggerath et al., 2011; NSC, 2006). The Essential Service Water Systems (ESWS) are used to provide cooling water to the safety-related equipment that must function during and following an accident, and consist of different components that may vary with the characteristics of each plant. In the 1999 Blayais Nuclear Power Plant flood the safety of the plant was endangered because of a partial failure of some ESWS pumps (Mattei et al., 2001) and these systems were totally destroyed during the Fukushima accidents in 2011 (Funabashi and Kitazawa, 2012).

The safety level of the ESWS can be increased by means of redundant systems. For the study case presented in this paper, this additional emergency system is composed of an elevated water tank or reservoir, at a much higher altitude than the plant itself, and series of pipes that can supply water for cooling driven only by gravity to the different groups. In this way, the ESWS can work for a sufficiently long time

* Corresponding author.
Email address: marcos.sanz-ramos@upc.edu (M. Sanz-Ramos)

https://doi.org/10.1016/j.nucengdes.2019.110180
Received 10 October 2018; Received in revised form 20 June 2019; Accepted 28 June 2019
Available online xxx
0029-5493/

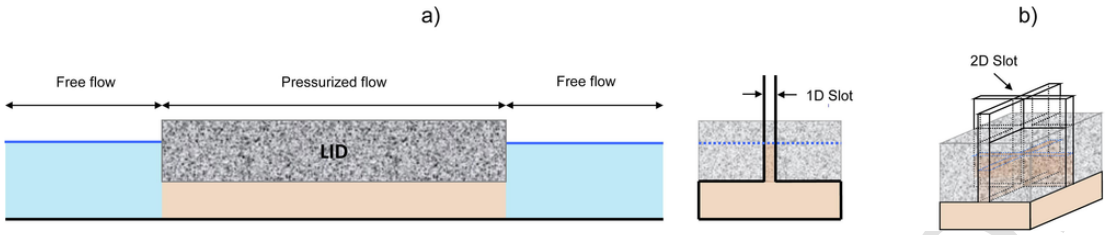

Fig. 1. Scheme of pressurized flow using the Preissmann Slot Method in 1D (a) and 2D (b).

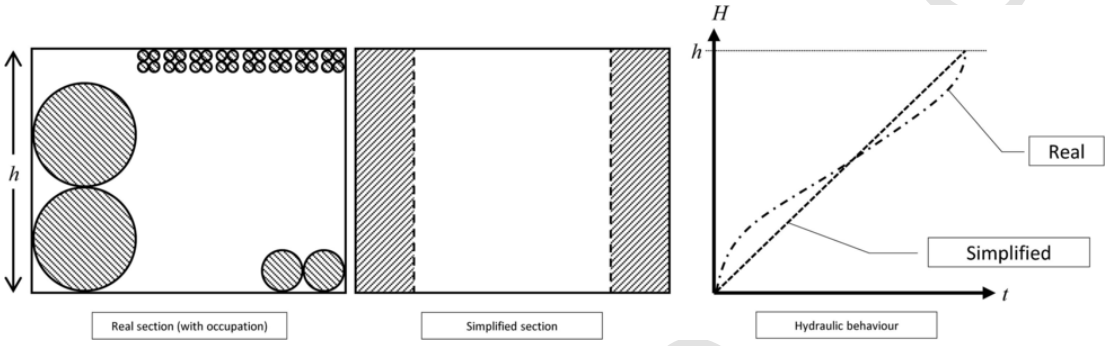

Fig. 2. Representation of a service gallery cross section occupied with pipes and elements (left), its approximation as considered by the numerical model (centre) and its effect on the filling process as implemented in the model.

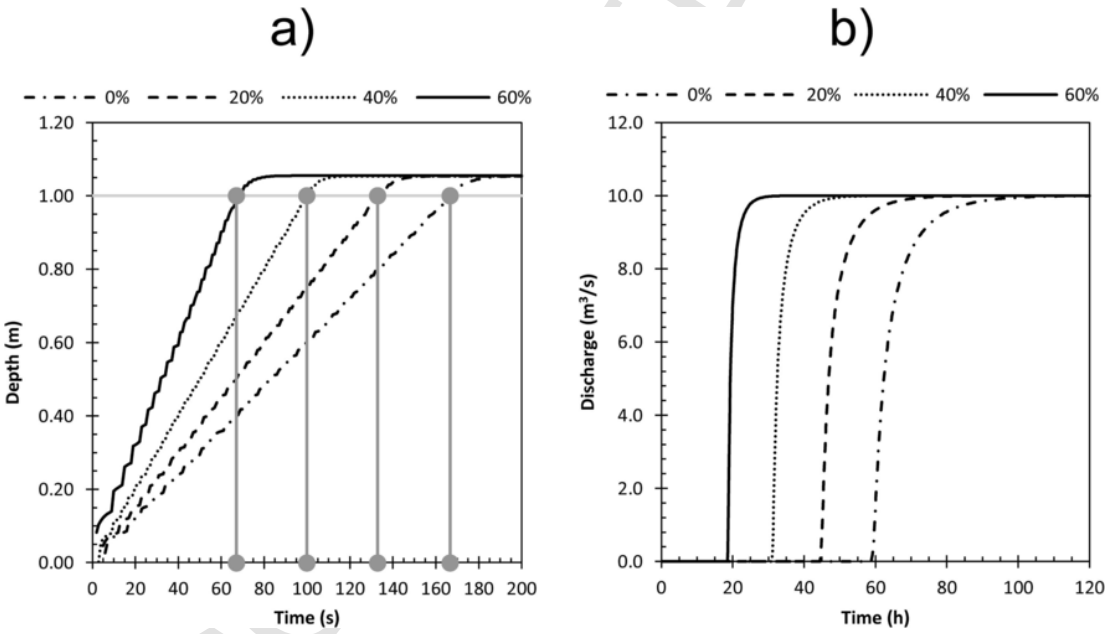

Fig. 3. Verification process: a) comparison of the time elapsed during the filling process of a rectangular channel compared with the theoretical value for a depth of 1 m and b) discharge/time curves at the outlet of the channel with different occupations showing the flow acceleration caused by a cross section reduction.

even with a total loss of any power source. These ESWS pipes run along underground galleries, where they share space with other infrastructure (communication systems, other conduits, support elements, etc.). Depending on the number of elements occupying the galleries, the actual area of a gallery cross-section can be much smaller than its total area if there were no conduits. The pipes are an additional safety system, but if they happen to fail, water from the system might be released into the galleries, which could be flooded and behave as channels transporting water along them. In such case, various essential services could be affected, compromising the safety of the plant.

The present study focuses on the analysis of the inundation process of the gallery system due to the failure of the aforementioned ESWS pipes. The complexity of the geometry of the whole system (different bottom elevation at different points, steps, entrance/exit of pipes, lidded areas, isolated channels connected through culverts, intermediate walls, weirs, etc.) encourages the use of advanced numerical methods in preference to more simple numerical tools or other alternatives such as scaled physical hydraulic models.

Since the 1980s, hydraulic numerical models have significantly improved from simple one-dimensional models of channels to three-dimensional approaches including turbulence models. The latter are presently used for complex flows in limited spatial domains such as water flow around bridge piers. Among the possible numerical strategies capable of properly reproducing the hydraulic behaviour of the flow inside the NPPs service galleries with affordable computational

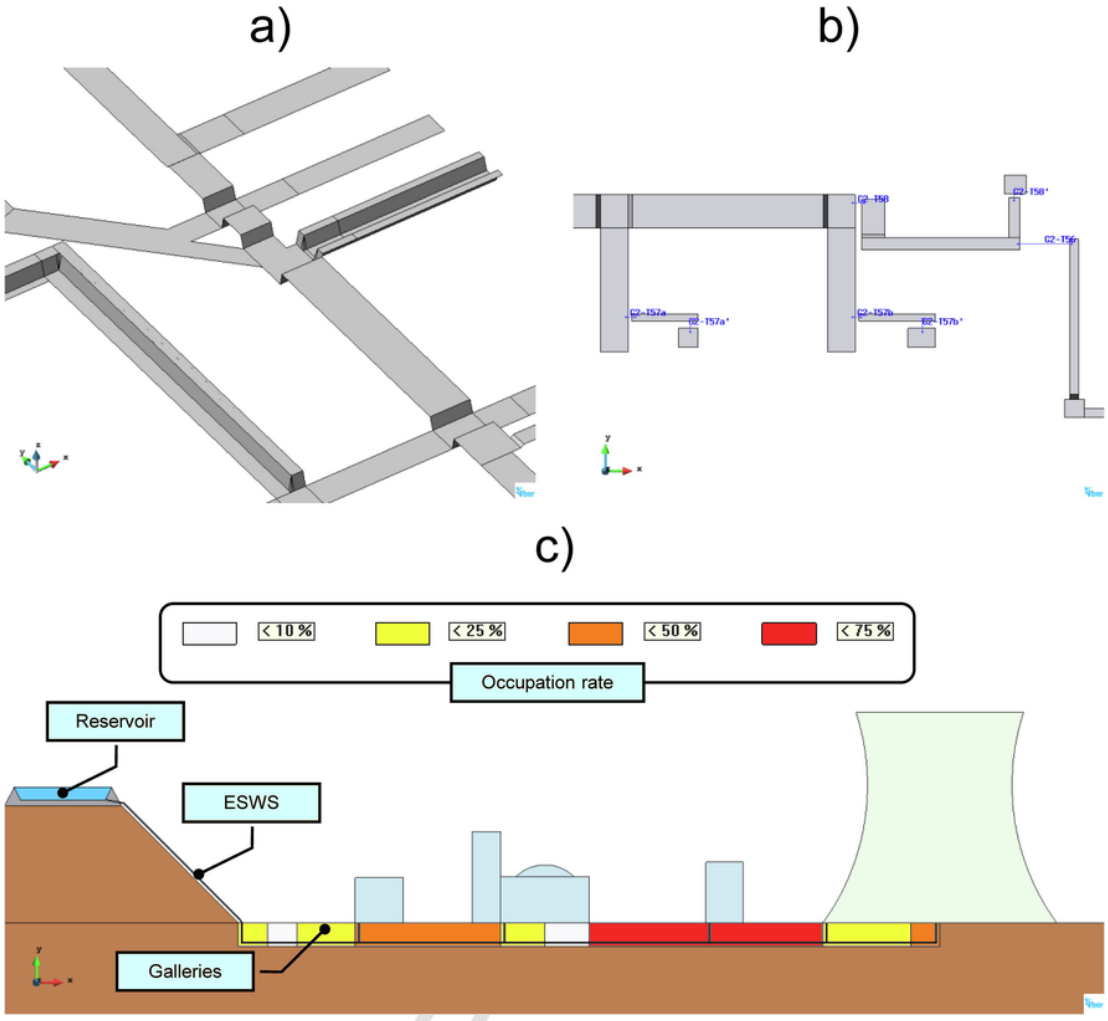

Fig. 4. Schematic representation of the service galleries. a) 3D visualization showing cross-section, bottom elevation and alignment changes; b) plan view of isolated channels linked by close conduits and c) general scheme of the ESWS running along the service galleries.

Table 1
Values and characteristics of the discharges in the six breaking points.

	P1	P2	P3	P4	P5	P6
Section [mm^2]	70685.8	49087.4	70685.8	1311	70685.8	943.1
Length [m]	441.03	451.19	634.61	634.61	983.62	451.19
Lambda	11.5	13.7	11.34	11.34	16.34	13.7
f	0.0223	0.0234	0.0223	0.0223	0.0223	0.0234
Discharge [m^3/s]	**0.329**	**0.204**	**0.287**	**0.025**	**0.233**	**0.018**

cost, two-dimensional (2D) models are presently an efficient option that can provide detailed and high resolution results.

There are a good number of commercial hydraulic modelling tools capable of simulating unsteady open channel flow in variable and irregular cross-section channels with complex geometries. When choosing one, there are three aspects that, in the present case, are a determining factor: i) the presence of reaches with pressurized flow, ii) the existence of isolated channels connected to the main galleries through closed conduits and iii) the aforementioned occupation of the galleries by different services (pipes, supports, etc.). The effect of the last one is a significant modification of the conveyance capacity of the whole system due the reduction of the available space for the water flow. In channels with high occupation, water fills the channels faster than in the case of a non-occupied channel. Most recent tools for numerical modelling of Computational Fluid Dynamics and open channel flow, either in two or three dimensions, are based on the finite volume method (Bermúdez Pita, 2013; Knight, 2013), although recently the Smooth Particle Hydrodynamics method (SPH) has shown also good performance for three dimensional computations (Liang et al., 2015; López et al., 2010). Nevertheless, for the present case, we chose the two dimensional approach because of the complexity and large dimensions of the area.

The tool used to perform the numerical simulations was Iber (Bladé et al., 2014b), a high resolution advanced two-dimensional modelling tool for open channel flow. For the present study, new numerical capabilities were developed and added to the previously existing solver, and were verified in order to consider the effect of the occupation of the galleries in the propagation of the flood. The resulting new tool was applied to the study case, the main objective being the evaluation of the time elapsing between failure of the pipes and the instant at which the water elevation reaches a critical value at various control points.

In order to illustrate the relevance of the numerical developments presented here, the results of the numerical model obtained with the real geometry (with occupation) were compared with those obtained considering no occupation of the galleries at all (full section available for water flow). It will be seen that the results differ significantly, and if the gallery occupation is not properly considered, as could happen if more traditional hydraulic numerical models were used, they can be on

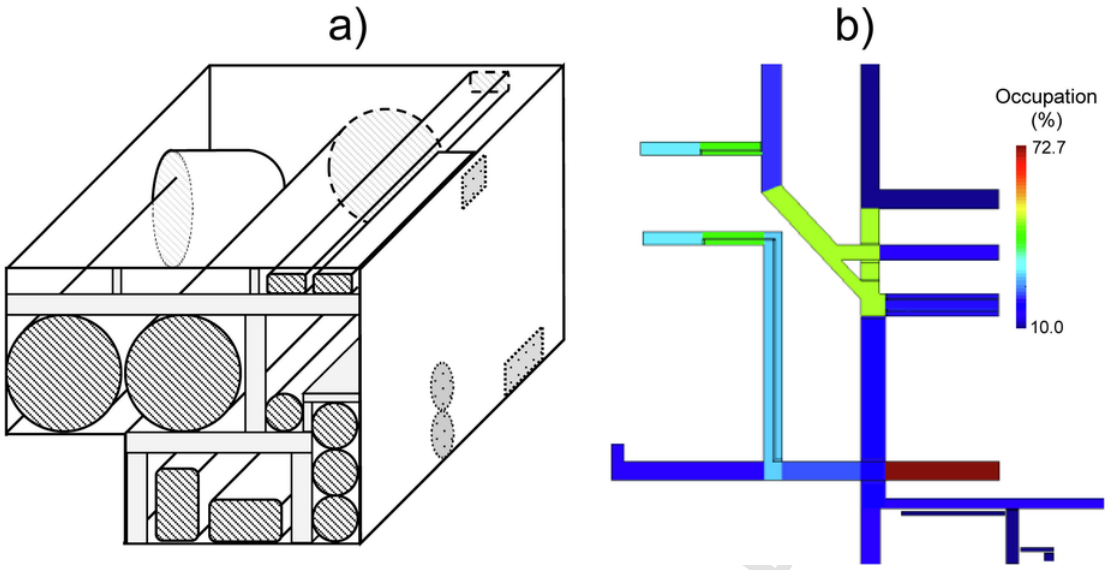

Fig. 5. Occupation: a) Sketch of a service gallery where the shadow parts represent the entry and exit of some elements; and b) representation of the occupation index in the numerical model.

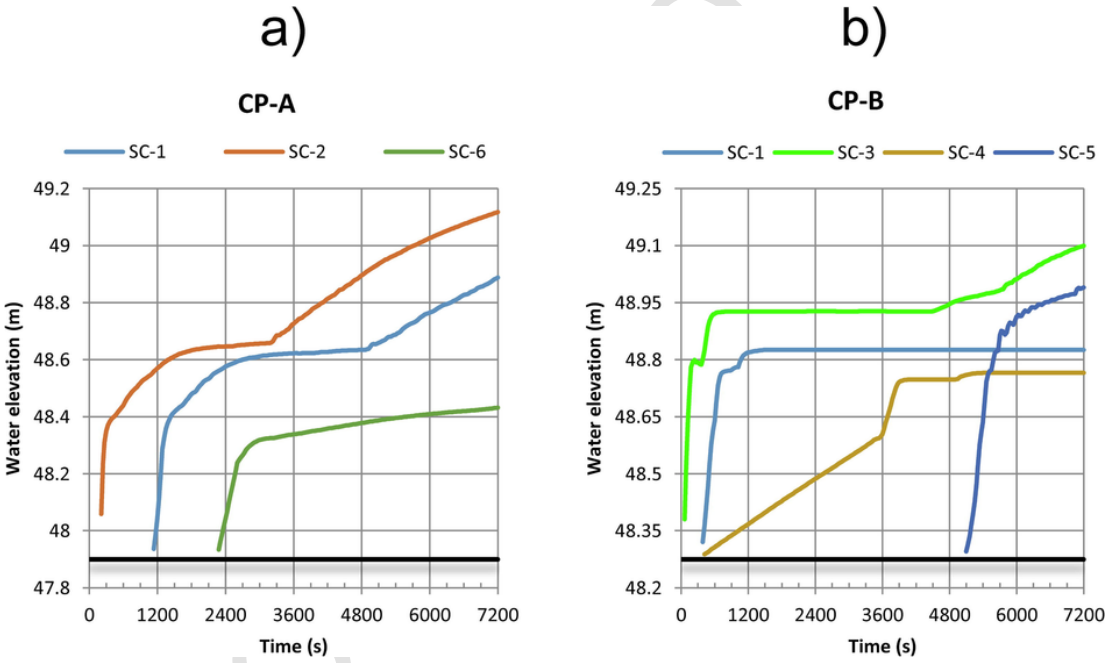

Fig. 6. Example of the results obtained. Water evolution for the six scenarios at two control points (CP-A and CP-B).

the unsafe side. For some of the studied scenarios, the difference in the time taken by the water to reach the critical level at some control points is more than 20 min.

2. Methods and materials

2.1. Numerical model

Nowadays numerical simulation is a useful and powerful tool to analyse and predict physical processes such as industrial forming processes (Ryzhakov et al., 2016), structural analysis (Barbu et al., 2015; Chacón et al., 2016), electromagnetic interference (Otin, 2013), fluid dynamics (Bussetta et al., 2014; Colomés et al., 2016), etc. Using numerical models, it is possible to minimize and in some cases avoid experimental studies, and it is also possible to understand complex phenomena for which direct observation and measuring is difficult or impossible (Jeong et al., 2017; Mimouni et al., 2016). Numerical modelling has been widely used in flood analysis and management. With it, it is possible to evaluate the extension of inundation areas to describe the flow velocities and discharge fields and, in consequence, to plan strategies oriented to reduce the flood risk (Bladé et al., 2014a; Chen et al., 2017; Sopelana et al., 2018).

Iber is a free two-dimensional (2D) hydraulic software developed in cooperation by three research groups (Flumen Institute of Universitat Politècnica de Catalunya, GEAMA group of Universidade da Coruña and CIMNE, the International Centre for Numerical Methods and Engineering). Iber is distributed through www.iberaula.com. Its main hydrodynamic module solves the 2D Saint Venant equations, or Shallow Water Equations (2D-SWE), which are derived from the Navier–Stokes equations after temporal averaging, in order to filtrate the turbulent

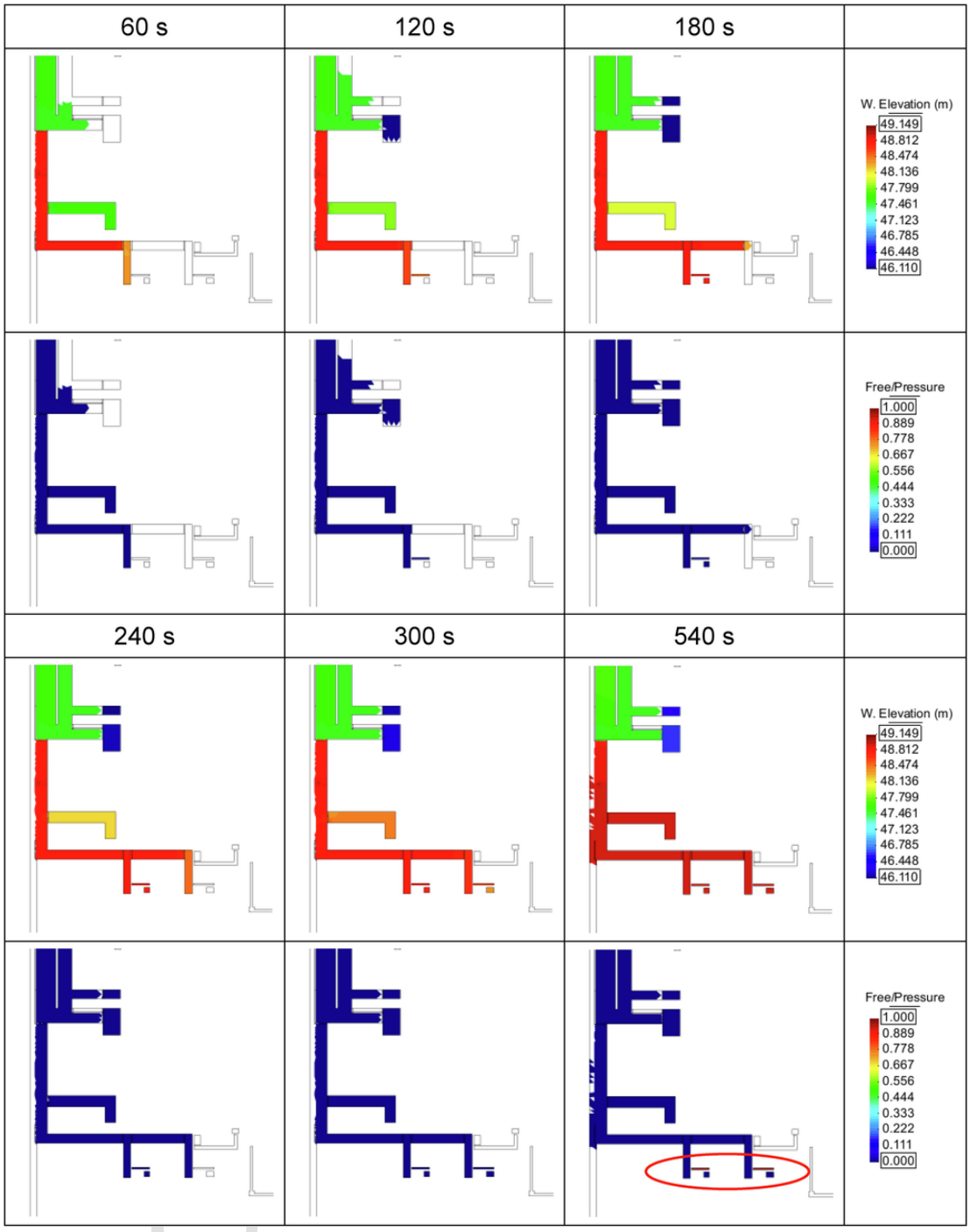

Fig. 7. Flood evolution considering guillotine-type failure of ESWS. Water elevation map (top) and free/pressure map (bottom) for 6 instants in the first 9 min of simulation (results each minute, except of 540 s time-step) in a small area of the gallery system.

fluctuations (leading to the Reynolds equations), and depth averaging, to transform the three-dimensional equations to two-dimensional (Tan, 1992; Toro, 2009). These equations assume hydrostatic pressure distribution and predominant horizontal dimensions over the vertical one. 2D-SWE are a non-linear hyperbolic system of differential equations, and can be written, in conservative form, as:

$$\frac{\delta h}{\delta t} + \frac{\delta h U_x}{\delta x} + \frac{\delta h U_y}{\delta y} = 0 \tag{1}$$

$$\frac{\delta h U_x}{\delta t} + \frac{\delta h U_x^2}{\delta x} + \frac{\delta h U_x U_y}{\delta y} = gh\left(S_{o,x} - S_{f,x}\right) \tag{2}$$

$$\frac{\delta h U_y}{\delta t} + \frac{\delta h U_x U_y}{\delta x} + \frac{\delta h U_y^2}{\delta y} = gh\left(S_{o,y} - S_{f,y}\right) \tag{3}$$

where (1) represents mass conservation while (2) and (3) are the momentum equations in the two horizontal X and Y directions. In these

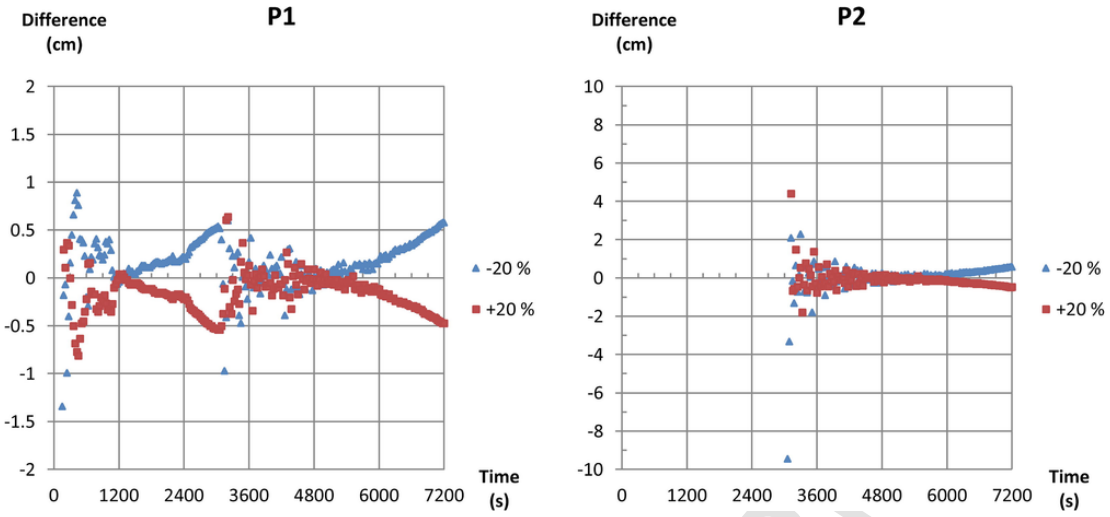

Fig. 8. Sensitivity analysis. Evolution of the water elevation difference (cm) among the 0.0144 $s \cdot m^{-1/3}$ (−20%) and 0.0216 $s \cdot m^{-1/3}$ (+20%) roughness coefficient cases versus the value chosen for the study (0.018 $s \cdot m^{-1/3}$).

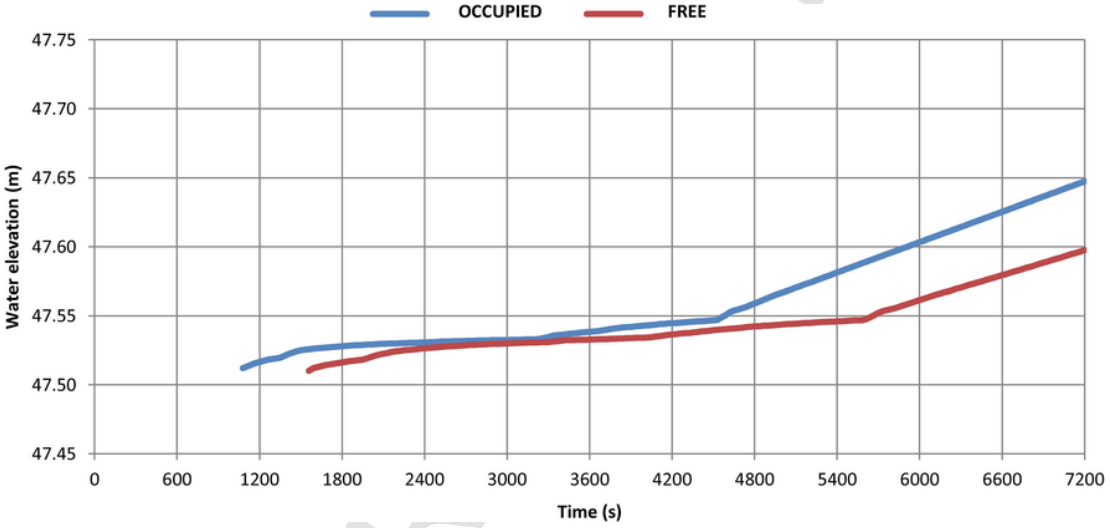

Fig. 9. Occupation sensitivity analysis. Evolution of water elevation.

equations, h is the depth, U_x and U_y are the two horizontal components of the depth-averaged velocity, g is the gravity acceleration, S_o is the bed slope (4) and S_f is the friction slope, here evaluated with the Manning formula (5).

$$S_{o,x} = -\frac{\delta z_b}{\delta x} \quad S_{o,y} = -\frac{\delta z_b}{\delta y} \tag{4}$$

$$\tau_{b,x} = \rho g h \frac{n^2 |\boldsymbol{U}| U_x}{h^{4/3}} \quad \tau_{b,y} = \rho g h \frac{n^2 |\boldsymbol{U}| U_y}{h^{4/3}} \tag{5}$$

In (4) and (5) z_b is the bottom elevation, n is the Manning coefficient and $|\boldsymbol{U}|$ is the module of the velocity ($|\boldsymbol{U}| = \sqrt{U_x^2 + U_y^2}$). The solver used in Iber is a Godunov-type scheme based on the Finite Volume Method (FVM) that uses the Roe Approximate Riemann Solver (Cea et al., 2016; Cea and Vázquez-Cendón, 2009; LeVeque, 2002; Toro, 2009; Vázquez-Cendón, 1999). In this type of explicit numerical scheme, the computational time-step is limited by the Courant–Friedrichs–Lewy (CFL) condition (Courant et al., 1967) and thus computational times are a relevant factor. The versatility of the numerical method and the scheme implemented in Iber facilitates the development of new tools and methodologies for simulating other 2D hydraulic phenomena. The implementation in Iber of the numerical schemes, as well as verification against analytical solutions, experimental data, and benchmark cases is detailed in Bladé (2005) and Cea (2005).

2.1.1. Numerical solvers

In order to simulate the complex hydraulics of the case study, apart from the basic open channel flow module, four additional specific numerical modules of Iber were used:

- *Culverts*. They allow transferring water from one point of the computational mesh to another one by means of a close conduit.
- *Lids*. A module to simulate pressurized flow, even though the general approach is that of a 2D free surface model.
- *Sources*. They provide the possibility of introducing water, with constant or variable discharge, punctually inside the model.
- *Channel occupation*. This module uses modified continuity and momentum equations with the aim to account for the effect of the different elements partially occupying the cross-section. It has been developed ad hoc for this study.

Of the previous modules, *culverts* are used to represent pipe connections between interrupted or different channels. The culvert tool calculates the discharge between two points from the difference in water elevation using the Manning formula (6):

$$Q = \frac{1}{n} A\hat{A} \cdot R_h^{2/3} \hat{A} \cdot S_f^{1/2} \tag{6}$$

where Q is the discharge, A is the wet area of the culvert, n is the Manning coefficient, R_h is the hydraulic radius and S_f is the friction slope or the gradient of the energy line, approximated here as the gradient of water elevation between the inlet and the end of the culvert. As the water level in the pipe ends changes gradually, and the maximum length of these pipes is of a few decimetres, the use of Eq. (6) is justified in this case.

Sections where the service galleries are covered, in which there might be pressurized flow instead of open channel flow, are calculated with the *lid* module which uses the Preissmann Slot method (Preissmann, 1961) to solve the full dynamic equations of pressure flow. This method approximates closed conduits as open channels with a lower wide section and an upper narrow hypothetic slot (Fig. 1a). As Iber is a two-dimensional tool, a cross-shaped slot (Fig. 1b) was used to extend the Preissmann Slot technique to two dimensions, as described by Aragón-Hernández and Bladé (2017).

The *source* tool allows the introduction of a water discharge inside the model at a specific point (mesh element). To do that, a new source term is added in the mass conservation Eq. (1) in order to modify the amount of water of the element.

Finally, the new *occupation* tool was developed for this study to simulate obstructions in cross-sections with a reduction of their original area due to the presence of different elements (Fig. 2). Hence, the volume available to the flow is reduced by the presence of elements inside the channel (or service gallery in our case). For this purpose, an *occupation index* (i_o) is defined as the ratio between the cross sectional area with occupation and without occupation. This index is included in the discretized form of the continuity Eq. (1) through a reduction coefficient ($\alpha = 1 - i_o$) that modifies the available volume in each finite volume according to Eq. (7):

$$h_i^{n+1} = h_i^n - \frac{\Delta t}{\alpha V_i} \sum_{k=1}^{n_l} Q_{i,k}^n \tag{7}$$

where h_i^{n+1} is the depth at time step $n + 1$, h_i^n the depth at time step n , $Q_{i,k}^n$ the discharge (mass flow) from finite volume i to finite volume k, n_l the number of sides of finite volume i, V_i its volume (or surface in a 2D approach as is the present case) and Δt the time steps between time step n and $n + 1$.

With this approach, even though the real occupation varies as a function of the distance to the bottom of the galleries, a mean occupation for the whole cross section is assumed. The occupation differences at different heights could be taken into account in Eq. (7) if α was considered to be dependent of the depth ($\alpha(h)$). Nevertheless, for the present study α was considered to be constant in each cross section (though varying from cross section to cross section) for two reasons: i) the high complexity and different disposition of elements in the galleries make it very expensive, in terms of personnel time, to include the occupation in such detail and ii) the option to use a mean occupation was on "the safe side" for the purpose of the study, as generally the pipes and elements are more near the top of the gallery than lying on its bottom. With such simplification, the real propagation of the water front will be slightly slower than the calculated one.

2.1.2. Validation

A verification process was performed for the new module *Occupation*. As previously stated, this module was designed to properly reproduce the reduction of the channel filling time before water reaches a control point due to the presence of elements in the service galleries.

For verification, four completely flat channels 3.33 m in length and 0.5 m wide were used. Each channel had a single occupation index along its whole length, which changes with steps of 20% from channel to channel, starting at 0% and with a maximum of 60%. The total volume of each channel was 1.667 m^3, 1.333 m^3, 1.000 m^3 and 0.667 m^3. With a constant flow rate of 0.01 m^3/s in the channel inlet and a weir in the outlet (1 m height), the theoretical filling times for each channel were 166.7 s, 133.3 s, 100.0 s and 66.7 s, respectively.

The first step was to corroborate that the simulated filling times are in concordance with the theoretical values as shown in Fig. 3a, where the time needed by the numerical model to reach a depth of 1 m is exactly the same that the time obtained by performing an analytical water volume balance.

The second verification consisted in checking the flow acceleration process due to a section reduction in a 50,000 m long and 50 m wide channel with a 0.1‰ slope. In the 30,000 m long central part four different occupation indexes (0, 20, 40 and 60%) were tested. The boundary conditions for that verification test were a flow rate of 10 m^3/s in the inlet, critical depth downstream, in order to have a unique depth-discharge relation, and 0.05 $s \cdot m^{-1/3}$ Manning roughness coefficient. Fig. 3b shows the flow hydrograph at the outlet, showing that the outlet point is reached earlier in the channels with more occupation, and also that less time is needed to achieve the steady state because of flow acceleration occurring due to the constriction effect caused by the section reduction.

2.2. Case study

The NPP object of the study is located in Spain. The plant has a complex underground system of service galleries with many pipes and conduits along the galleries going in and out of them. These galleries, which in our case are considered as channels, consist of different reaches, each of them with a horizontal bottom but different bottom elevations, and with different cross-section geometries (width and height). A schematic 3D representation of the galleries can be observed in Fig. 4a. The system mainly behaves as a continuous channel network, but some parts of the infrastructure remain isolated and are only connected with the rest of the system by small pipes (Fig. 4b). Concrete lids cover the whole network, but only some parts (under the roads and buildings) can be considered as fully closed channels, where pressure flow can take place. For the rest of them there are gaps between the concrete pieces that are used to cover the galleries where water can flow through. The ESWS runs along the galleries from an upper water reservoir to some specific locations of the NPP (Fig. 4c).

2.2.1. Discharges

The ESWS pipes are mainly located inside the gallery network, and share the space with other infrastructure. As previously stated, the purpose of these pipes is to supply water from an elevated reservoir to different parts of the NPP by means of two different pipes (Fig. 4c). For the case study, the reservoir has 10 m high dam, a storage volume up to 30,000 m^3 and is located 50 m above the main level of the galleries. At the upper part, the diameter of the two pipes is 300 mm, but once the pipes enter the galleries, the diameter of one of them changes to 250 mm.

In this study two different types of pipe failure were considered: a partial failure, or *crack* failure and a total pipe cross-section break, or *guillotine* break. Six different scenarios (P1 to P6) were studied, consist-

ing of two different locations for crack failure and four locations for full or guillotine break. The discharges spilling from the pipes through the broken sections are the inlet conditions for the simulations of the flood propagation along the galleries. These discharges spilling from the pipes depend on several factors, as the type of break, the distance between the breaking point and the reservoir (linear energy losses) and the type and number of elbows or direction changes of the pipe (local energy losses).

In the guillotine-type break the whole discharge transported by the pipes is released instantly into the galleries. The flow rate through a pipe can be evaluated by means of the energy conservation equation, or Bernoulli equation, which links the flow energy per unit of weight at different cross-sections of a pipe. Along the flow direction there are energy losses that are usually divided into linear losses due to friction, and local losses due to turbulent energy dissipation at some individual points such as contractions, expansions or elbows. Hence, by applying energy conservation between the reservoir and any point of the pipe system, the exit discharge of guillotine break scenarios can be obtained from Eq. (8):

$$H = \left[\frac{f}{\Phi}L + \sum \lambda + 1\right]\frac{Q^2}{2gA^2} \tag{8}$$

where H is the elevation difference between the reservoir water surface and the breaking point, f is the Darcy–Weisbach friction coefficient, θ is the diameter of the pipe (250–300 mm depending on the reach), L is the length of the pipe between the reservoir and the breaking point, λ is the addition of the energy loss coefficients at each contraction/expansion or elbow, g is the gravity acceleration, A is the pipe section and Q is the discharge.

Linear energy losses depend directly on the length of the pipe and the friction coefficient and are inversely proportional to the pipe diameter. The friction coefficient (f) can be evaluated by means of the Colebrook (1939) formula which, for fully turbulent flow, is equivalent to the second equation of Kármán–Prandtl (9):

$$\frac{1}{\sqrt{f}} = 1.14 + 2\log\frac{\theta}{k} \tag{9}$$

where k is the absolute roughness (0.5 mm).

In crack-type failure only a fraction of the discharge flowing through the pipes is spilt into the galleries, while the rest keeps flowing along them. In this case, the discharge can be evaluated with an iterative process involving the previous Eq. (9) and the equation of the flow across an orifice (10):

$$Q = C_d\hat{A}\cdot A\hat{A}\cdot\sqrt{2\hat{A}\cdot g\hat{A}\cdot H} \tag{10}$$

where C_d is a discharge coefficient and A_c is the area of the crack.

Table 1 presents the main values of the six scenarios calculated (P1 to P6). Breaking points 1, 3, 4 and 5 correspond to a 300 mm pipe-size, while points 2 and 6 to 250 mm pipe-size. The discharge for crack-type failure (P4, P6) is at least one order of magnitude lower than for a guillotine-type break (P1, P2, P3, P5), which means that the latter is much more critical in terms of available time to take any action after the break.

The values of the discharges at the breaking points for the different scenarios with the method explained above were obtained under the hypothesis of constant water elevation in the upstream reservoir. In this case it was a reasonable hypothesis because the maximum storage capacity of the galleries was around 8.000 m^3, which corresponds to a water elevation dropdown of the reservoir of 1.25 m, which is a relative small value compared with the difference between the elevation of the reservoir and the plant (around 50 m). Moreover, as the discharge is greater the greater this head is, the calculated discharges will be slightly larger than the real ones and thus this hypothesis is on the safe side. The highest point of the gallery channels is at an elevation of 49.95 m. If water reaches this elevation, it is spilt out from the system to the ground surface because 49.95 m is the maximum possible elevation of the free surface.

2.3. Model set up

The topographic data used to build the numerical model was provided in CAD format and was directly imported into Iber. This data consists of the definition of the channels in the XY plane, and their bottom elevation. The total length of the channels is slightly above 2 km. For simulation set up purposes, the channel network was divided into 122 reaches, each one with its own geometric characteristics (including occupation index and/or lids). A total of 64 reaches were covered (or lidded) areas. In addition, there were 46 culvert-type connections between the main channel net and isolated stretches (Fig. 4b).

The elements inside the channel network consisted mainly of pipes (ESWS and others) and electric and telecommunication cables and their supports (Fig. 5a). From the analysis of the conduits and supports in each channel reach, an occupation index (i_o) was assigned to all of them. To take into account the supports and other small elements different from pipes that exist in all galleries, a minimum value of 10% was used. The real occupation index was initially calculated considering only the pipes and conduits in the galleries, but then a multiplying factor of 1.25 was applied to i_0 to take into account the supports and other nonlinear elements, which are difficult to quantify in detail. With these considerations, the occupation index varies from 10% to 72.7% (Fig. 5b).

A non-structured triangular computational mesh was used to discretize the channel geometry. The mesh was generated from the geometry using the standard *Rfast* mesher of the Iber Interface, which is based on the GiD pre and post-processor software (CIMNE, 2011). The size of the elements (finite volumes) ranges between 0.001 and 1.17 m, with a total of 16,666 elements. The inlet conditions are, for each scenario, the discharges at the ESWS breaking points. For this condition, the *source* tool of the software was used. In this way, a volume of water equal to the specified discharge times the calculation time increment is added at each time step to the finite volume with inlet condition. An outlet weir boundary condition was assigned to the top of the gallery walls to consider that water going out from the galleries through the top cover gaps flows onto the ground surface, outside of the galleries. Water exiting to the ground surface was considered to leave the computational domain. For the lidded areas, there was no outlet condition. The roughness coefficient was set to 0.018 $s{\cdot}m^{-1/3}$ at the channel bottom and 0.015 $s{\cdot}m^{-1/3}$ at the walls. A zero depth (dry situation) initial condition was used in the whole domain. There were some points where the galleries were connected to the plant's drainage system, but in order to stay on the safe side, it was considered that the drainage system did not work, or that these connections did not exist.

3. Results and model sensitivity

3.1. Results

As previously said, six scenarios were studied considering two types of ESWS failure (crack and guillotine). The analysis of the results was done at 32 control points. In them the time between the pipe breaking and the arrival of the flood at the critical elevation (different for each control point) was evaluated. The model provides many different hydraulic results (evolution of water elevation, depth, velocities, dis-

charge, shear stress, Froude number, etc.), but for the present study the basic results were represented by means of the graphs of time evolution of water depths at control points. As shown in Fig. 6, the water elevation does not increase at a constant rate, not only because of complexity of the channel network but also to the channel occupation. This is an important point for the reaction time in case of failure.

As an example of the flooding process, Fig. 7 shows the water evolution for a guillotine-type failure (discharge of 0.287 m^3/s). It can be seen that between the time steps represented, there are some steps of the value of water elevation at specific locations. These are caused by the existence of very narrow cross sections, culverts or bottom elevation discontinuities which are translated into important localized water head losses. Furthermore, the inundation of some isolated channels can be observed. This is because of the presence of pipes connecting them to others, which were modelled with the culvert tool. Regarding the type of flow (free or pressurized), even though in the plotted area nine channels were completely closed (with lid), only in two of them pressurized flow did occur for time values greater than 540 s (highlighted by means of a red oval-line).

The time needed by the flow to reach a control point varied from 1 min to more than 2 h depending on the breaking point and on the control point location.

3.2. Sensitivity analysis

A sensitivity analysis to assess the influence of the bottom roughness (Manning coefficient, n) and occupation index (i_0) was carried out, as there are uncertainties in the evaluation of these values.

The effect of the Manning coefficient was analysed for the worst scenario: guillotine-type break of the pipes; breaking point close to the control points; and a middle–high discharge (0.204 m^3/s). Three models were built using Manning coefficients of 0.0144 $s \cdot m^{-1/3}$ (−20%), 0.018 $s \cdot m^{-1/3}$ and 0.0216 $s \cdot m^{-1/3}$ (+20%). Fig. 8 shows an example of the evolution of the water elevation at two control points for a ±20% variation of the Manning coefficient versus the value of 0.018 $s \cdot m^{-1/3}$. It can clearly be seen that in this case the Manning coefficient is not determinant, as differences of only a few centimetres were observed (less than 2 cm in most cases).

The influence of the occupation index was analysed by comparing the results of simulations with the occupation values used in the study with those considering no-occupation. The results presented here correspond to a scenario with a discharge of 0.287 m^3/s (guillotine-type break). The water elevation at a control point in both situations was compared (Fig. 9). In this case, with occupation the water front arrives at the control point (at an elevation of 47.60 m) approximately 20 min sooner than in the no-occupation scenario. A similar pattern is reproduced in the rest of the simulations, varying from few seconds to more than 20 min depending on the discharge and the closeness of the break-point and the control-point.

4. Conclusions

A methodology based on the combination of the two-dimensional shallow water model with the Finite Volume Method has been proved to be adequate to simulate the flooding of the service galleries of a nuclear power plant (NPP), even though the complexity of the geometry and hydraulic phenomena involved required the use and implementation of non-standard modules for two-dimensional free surface models. These modules are required for the simulation of special elements such as culverts (flow through pipes), lids (pressurized flow), sources (inlet discharge inside the model) and occupation (reduction of the effective cross-section area due to different elements).

For the study case, the origin of the flood was the hypothetical failure of the Emergency Service Water System (ESWS) pipes. This system runs along underground galleries with complex geometries.

The model with extended capabilities was first verified and then used in the case study. Two kinds of channel were used in the verification process. In both cases the results showed that the computed faster filling of the channel and acceleration of the flow (lower flow front arrival times) in reaches with significant occupation fitted with the theoretically expected values.

The methodology was applied in order to describe and analyse the process of flooding of the service galleries of a NPP. For plant managers, the most relevant result of the simulations was the time needed for the flow to reach some specified control points defined by their X, Y and Z coordinates. This time depends on the location and type of the ESWS failure, but it could be observed that the occupation index had a relevant influence on the results. Some channels had occupation indexes greater than 70%. The results showed that the difference in the time gap between the failure and the arrival at the control point, calculated considering the channels with and without occupation, was greater than 20 min at some control points.

In conclusion, it has been seen that standard hydraulic numerical modelling tools, based on the solution of the Saint Venant equations in one or two dimensions are not adequate to analyse the inundation process of complex systems of the type of usual NPP service galleries. A diagnostic on the hazard related to the failure of the ESWS with such standard tools would most probably be on the safe side.

Nevertheless, 2D hydrodynamic modelling tools can be the basis for the aforementioned analysis, provided they are enhanced with additional tools as was done for the presented case study. Different study case might require different enhancements, but it has been seen that the modules specifically developed for this case (culverts, lids, occupation and punctual sources) are enough for the analysis of a significantly complex gallery system. For that reason, the presented methodology and newly developed tools could most probably be used as the base for similar stress tests at other NPPs.

Acknowledgement

The authors want to thank IDOM S.A. for all the collaboration and support during the study itself and the preparation of the article.

Appendix A. Supplementary data

Supplementary data to this article can be found online at https://doi.org/10.1016/j.nucengdes.2019.110180.

References

Aragón-Hernández, J.L., Bladé, E., 2017. Modelación numérica de flujo mixto en conductos cerrados con esquemas en volúmenes finitos. Tecnol. y Ciencias del Agua VIII, 127–142.

Barbu, L.G., Oller, S., Martinez, X., Barbat, A., 2015. High cycle fatigue simulation: a new stepwise load-advancing strategy. Eng. Struct. 97, 118–129. https://doi.org/10.1016/j.engstruct.2015.04.012.

Bermúdez Pita, M., 2013. Evaluación hidráulica y biológica de diseños de escalas de peces de hendidura vertical para especies de baja capacidad natatoria. Universidade da Coruña, Tesis UdC.

Bladé, E., 2005. Modelación del flujo en lámina libre sobre cauces naturales. Análisis integrado con esquemas en volúmenes finitos en una y dos dimensiones. Universitat Politècnica de Catalunya.

Bladé, E., Cea, L., Corestein, G., 2014. Numerical modelling of river inundations. Ing. del agua 18, 68. https://doi.org/10.4995/ia.2014.3144.

Bladé, E., Cea, L., Corestein, G., Escolano, E., Puertas, J., Vázquez-Cendón, E., Dolz, J., Coll, A., 2014. Iber: herramienta de simulación numérica del flujo en ríos. Rev. Int. Métodos Numéricos para Cálculo y Diseño en Ing. 30, 1–10. https://doi.org/10.1016/j.rimni.2012.07.004.

Bunn, M., Heinonen, O., 2011. Preventing the Next Fukushima. Science 333, 1580–1581. https://doi.org/10.1126/science.1209668.

Bussetta, P., Dialami, N., Boman, R., Chiumenti, M., Agelet De Saracibar, C., Cervera, M., Ponthot, J.P., 2014. Comparison of a fluid and a solid approach for the numerical simulation of friction stir welding with a non-cylindrical pin. Steel Res. Int. 85, 968–979. https://doi.org/10.1002/srin.201300182.

Cea, L., 2005. An Unstructured Finite Volume Model for Unsteady Turbulent Shallow Water Flow with Wet-dry Fronts: Numerical Solver and Experimental Validation. Universidad da Coruña.

Cea, L., Bermudez, M., Puertas, J., Bladé, E., Corestein, G., Escolano, E., Conde, A., Bockelmann-Evans, B., Ahmadian, R., 2016. IberWQ: new simulation tool for 2D water quality modelling in rivers and shallow estuaries. J. Hydroinform. 18, 816–830. https://doi.org/10.2166/hydro.2016.235.

Cea, L., Vázquez-Cendón, M.E., 2009. Unstructured finite volume discretization of two-dimensional depth-averaged shallow water equations with porosity. Int. J. Numer. Meth. Fluids 63, 903–930. https://doi.org/10.1002/fld.2107.

Chacón, R., Uribe, N., Oller, S., 2016. Numerical validation of the incremental launching method of a steel bridge through a small-scale experimental study. Exp. Tech. 40, 333–346. https://doi.org/10.1007/s40799-016-0037-5.

Chen, X., Ji, P., Wu, Y., Zhao, Y., Zeng, L., 2017. Coupling simulation of overland flooding and underground network drainage in a coastal nuclear power plant. Nucl. Eng. Des. 325, 129–134. https://doi.org/10.1016/j.nucengdes.2017.09.028.

Chiang, Y., Chen, S., Wang, J., Wang, T., Chen, H., Hsu, W., Chiang, S., Shih, C., 2017. Code crosswalk of Fukushima-like simulations for Chinshan BWR/4 NPP using MELCOR2. 1/SNAP, TRACE/SNAP, PCTRAN and MAAP5. 03. Nucl. Eng. Des. 325, 12–24. https://doi.org/10.1016/j.nucengdes.2017.09.023.

CIMNE, 2011. GID: The personal pre and postprocessor. Reference Manual. [WWW Document]. URL www.gidhome.com (accessed 6.20.19).

Colebrook, C.F., 1939. Turbulent flow in pipes, with particular reference to the transition region between smooth and rough pipe laws. J. Inst. Civ. Eng. 11, 133–156.

Colomés, O., Badia, S., Principe, J., 2016. Mixed finite element methods with convection stabilization for the large eddy simulation of incompressible turbulent flows. Comput. Meth. Appl. Mech. Eng. 304, 294–318. https://doi.org/10.1016/j.cma.2016.02.026.

COM, 2012. Communication from the Commission to the Council and the European Parliament on the comprehensive risk and safety assessments ("stress tests") of nuclear power plants in the European Union and related activities. European Commission. COM(2012) 571 final. Brussels, 4.10.2012.

Courant, R., Friedrichs, K., Lewy, H., 1967. On the partial difference equations of mathematical physics. IBM J. Res. Dev. 11, 215–234.

D'Auria, F., Debrecin, N., Glaeser, H., 2017. Strengthening nuclear reactor safety and analysis. Nucl. Eng. Des. 324, 209–219. https://doi.org/10.1016/j.nucengdes.2017.09.008.

Funabashi, Y., Kitazawa, K., 2012. Fukushima in review: a complex disaster, a disastrous response. Bull. At. Sci. 68, 9–21. https://doi.org/10.1177/0096340212440359.

Jeong, J.H., Song, M.S., Lee, K.L., 2017. CFD investigation of three-dimensional flow phenomena in a JAEA 127-pin wire-wrapped fuel assembly. Nucl. Eng. Des. 323, 166–184. https://doi.org/10.1016/j.nucengdes.2017.08.008.

Knight, D.W., 2013. River hydraulics – a view from midstream. J. Hydraul. Res. 51, 2–18. https://doi.org/10.1080/00221686.2012.749431.

LeVeque, R.L., 2002. Finite volume methods for hyperbolic problems. Cambridge Texts Appl. Math. 31.

Liang, Q., Xia, X., Hou, J., 2015. Efficient urban flood simulation using a GPU-accelerated SPH model. Environ. Earth Sci. 74, 7285–7294. https://doi.org/10.1007/s12665-015-4753-4.

López, D., Marivela, R., Garrote, L., 2010. Smoothed particle hydrodynamics model applied to hydraulic structures: a hydraulic jump test case. J. Hydraul. Res. 48, 142–158. https://doi.org/10.1080/00221686.2010.9641255.

Mattei, J.M., Vial, E., Rebour, V., Gorbatchev, A., 2001. Generic results and conclusions of re-evaluating the flooding protection in French and German nuclear power plants, Eurosafe. Eurosafe 2001 Paris (France) 5-6 Nov 2001; INIS-FR--1069 (INISFR1069).

Mimouni, S., Baudry, C., Guingo, M., Lavieville, J., Merigoux, N., Mechitoua, N., 2016. Computational multi-fluid dynamics predictions of critical heat flux in boiling flow. Nucl. Eng. Des. 299, 28–36. https://doi.org/10.1016/j.nucengdes.2015.07.017.

NERH, 2011. Report of Japanese Government to the IAEA Ministerial Conference on Nuclear Safety. The Accident at TEPCO's Fukushima Nuclear Power Stations. Nuclear Emergency Response Headquarters. Government of Japan. June 2011.

Nöggerath, J., Geller, R.J., Gusiakov, V.K., 2011. Fukushima: the myth of safety, the reality of geoscience. Bull. At. Sci. 67, 37–46. https://doi.org/10.1177/0096340211421607.

NSC, 2006. Regulatory Guide for Reviewing Seismic Design of Nuclear Power Reactor Facilities. Nuclear Safety Commission. September 2006.

Otin, R., 2013. A numerical model for the search of the optimum frequency in electromagnetic metal forming. Int. J. Solids Struct. 50, 1605–1612. https://doi.org/10.1016/j.ijsolstr.2013.01.023.

Preissmann, A., 1961. Propagation des intumescences dans les canaux et rivières (pp., in: 1st Congrèss Association Francaise de Calcul, Grenoble, AFC, Paris, France, September. pp. 433–442.

Ryzhakov, P.B., García, J., Oñate, E., 2016. Lagrangian finite element model for the 3D simulation of glass forming processes. Comput. Struct. 177, 126–140. https://doi.org/10.1016/j.compstruc.2016.09.007.

Saji, G., 2014. Safety goals for seismic and tsunami risks: lessons learned from the Fukushima Daiichi disaster. Nucl. Eng. Des. 280, 449–463. https://doi.org/10.1016/j.nucengdes.2014.09.013.

Sopelana, J., Cea, L., Ruano, S., 2018. A continuous simulation approach for the estimation of extreme flood inundation in coastal river reaches affected by meso- and macrotides. Nat. Hazards 93, 1337–1358. https://doi.org/10.1007/s11069-018-3360-6.

Tan, W., 1992. Shallow Water Hydrodynamics, first ed. Elsevier Science.

Toro, E.F., 2009. In: Riemann Solvers and Numerical Methods for Fluid Dynamics. Springer, Berlin (Heidelberg), https://doi.org/10.1007/b79761.

USNRC, 2011. Design-Basis Flood Estimation for Site Characterization at Nuclear Power Plants in the United States of America, NUREG/CR-7046. United States Nuclear Regulatory Commission. Pacific Northwest National Laboratory, Richland, USA, November 2011.

Vázquez-Cendón, M.E., 1999. Improved treatment of source terms in upwind schemes for the shallow water equations in channels with irregular geometry. J. Comput. Phys. 148, 497–526.

Wang, Q., Chen, X., 2012. Regulatory failures for nuclear safety – the bad example of Japan – implication for the rest of world. Renew. Sustain. Energy Rev. 16, 2610–2617. https://doi.org/10.1016/j.rser.2012.01.033.